INTERNATIONAL JOURNAL FOR NUMERICAL METHODS IN FLUIDS
Int. J. Numer. Meth. Fluids 2005; **47**:517–541
Published online 14 December 2004 in Wiley InterScience (www.interscience.wiley.com). DOI: 10.1002/fld.828

Multigrid acceleration for transonic aerodynamic flow simulations based on a hierarchical formulation

Mohamed Hafez*,† and Essam Wahba

Department of Mechanical and Aeronautical Engineering, University of California, Davis CA 95616, U.S.A.

SUMMARY

In a companion paper, the authors used a hierarchical formulation based on a Helmholtz velocity decomposition to simulate transonic flows over airfoils. The potential flow formulation is augmented with entropy and vorticity corrections and the numerical results are compared to standard Euler and Navier–Stokes calculations. For many aerodynamic applications, the corrections are limited to relatively small regions; the flow in the near and far fields is irrotational and isentropic. The entropy and vorticity corrections are governed by convection/diffusion equations while the non-homogeneous potential equation is of mixed type; elliptic in the subsonic domain and hyperbolic in the supersonic one. The forcing function represents the necessary correction for mass conservation. Upwind schemes are used for the convection terms of the scalar equations of the corrections and for the potential equation in the supersonic region. The formulation can be viewed as an implementation of a viscous/inviscid interaction procedure which is equivalent to Navier–Stokes equations in the inner field.

In this paper, convergence acceleration techniques are applied for such a formulation using single and multiple grids. For a single grid, optimal relaxation parameters for subsonic potential flow regions and local artificial time steps for the scalar correction equations have been used. A full multigrid technique is implemented to the augmented potential equation. Only three grids: coarse, intermediate and fine meshes are used. Results for both inviscid and viscous transonic flows are presented. It is noticed that the potential and the viscous flow calculations, based on the present formulation, have comparable convergence histories. The limited applications of multigrid result in an order of magnitude saving of the work units for both calculations. More savings should be achievable with more sophisticated multigrid procedures. Copyright © 2004 John Wiley & Sons, Ltd.

KEY WORDS: transonic flow; multigrid acceleration

1. INTRODUCTION

In the last three decades, multigrid convergence acceleration techniques have been used in computational fluid dynamics. It has been proven to be a very effective tool for elliptic prob-

*Correspondence to: M. Hafez, Department of Mechanical and Aeronautical Engineering, University of California, Davis CA 95616, U.S.A.
†E-mail: mhafez@ucdavis.edu

Received 28 January 2004
Revised 16 July 2004

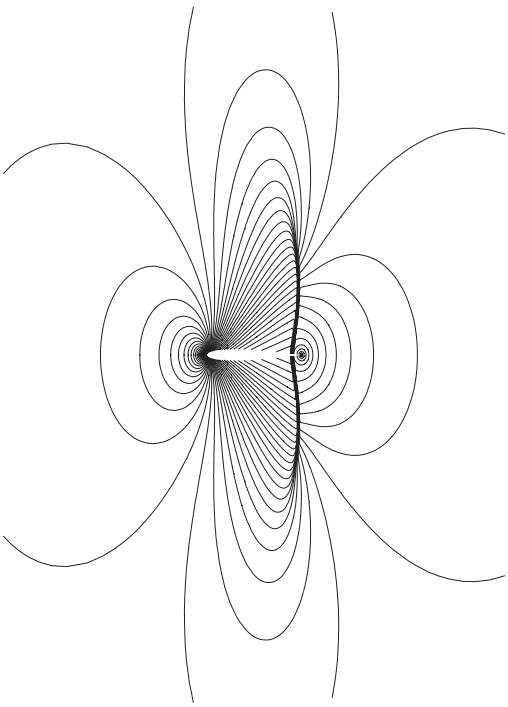

Figure 1. Mach contours ($M_\infty = 0.86$, potential flow, $\alpha = 0°$).

lems. Applications to flow simulations, governed by more complicated equations have been advocated by A. Brandt. His early ideas were summarized in Reference [1]. Since then, progress has been made by many researchers. Recently, textbook multigrid efficiency has been obtained by Thomas *et al.* [2]. Very impressive results for two-dimensional transonic inviscid flows are reported in Reference [3] by Caughey and Jameson. They used LU factorization with local iterations, rather than Runge–Kutta schemes adopted earlier in Reference [4], as a smoothing operator. Further investigations are, however, needed for viscous flow problems.

In the present paper, convergence acceleration techniques are applied for transonic aerodynamic steady flow simulations based on the hierarchical formulation of Reference [5]. The full multigrid procedure is applied to accelerate the convergence of iterative line relaxation methods to a steady-state solution of a potential equation (with non-homogeneous terms). Only three grids (coarse, intermediate and fine) are used. The calculations start with uniform flow as an initial guess for the coarse mesh. Mesh refinement is adopted to obtain a good initial guess for the fine mesh calculations. Multigrid is then applied with a V-cycle and standard restriction and prolongation schemes. The non-homogeneous terms are updated only on the fine mesh through solving scalar equations for the corrections to the potential field. The density is calculated in terms of the speed, augmented with entropy.

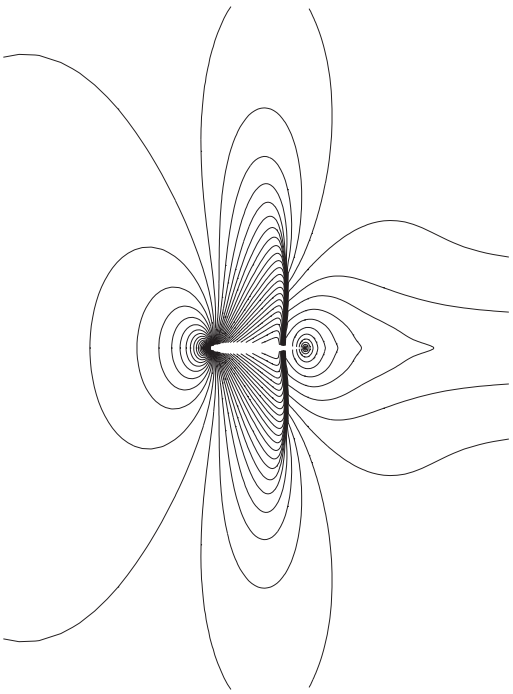

Figure 2. Mach contours ($M_\infty = 0.86$, rotational flow, $\alpha = 0^\circ$).

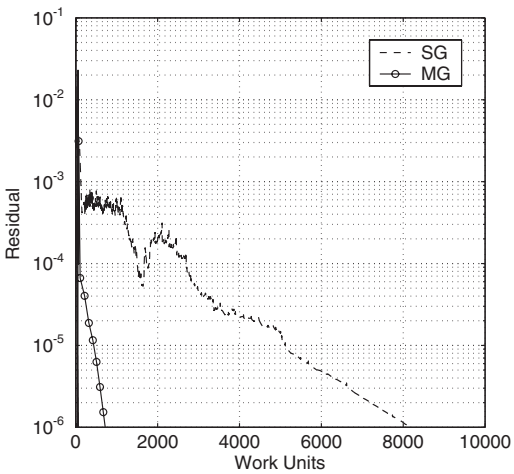

Figure 3. Convergence history ($M_\infty = 0.86$, potential flow, $\alpha = 0^\circ$).

Numerical results for inviscid and viscous flows with single and multiple grids are presented. The results of standard potential flow calculations (i.e. without corrections) are comparable to the early work of Jameson where he introduced the MAD scheme, see Reference [6]. On

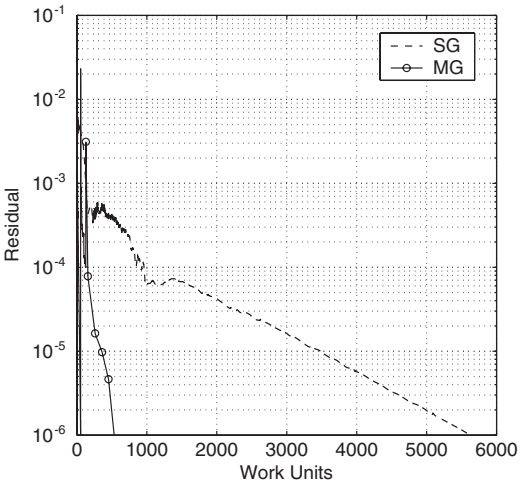

Figure 4. Convergence history ($M_\infty = 0.86$, rotational flow, $\alpha = 0^\circ$).

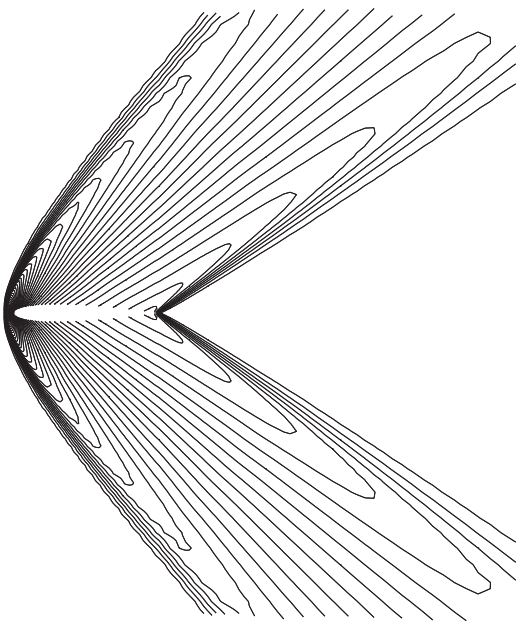

Figure 5. Mach contours ($M_\infty = 1.5$, potential flow, $\alpha = 0^\circ$).

the other hand, for viscous flow problems, the efficiency of the present results is comparable to that of Reference [7].

In the following, the details of the governing equations and the numerical methods are given and then the numerical results are discussed.

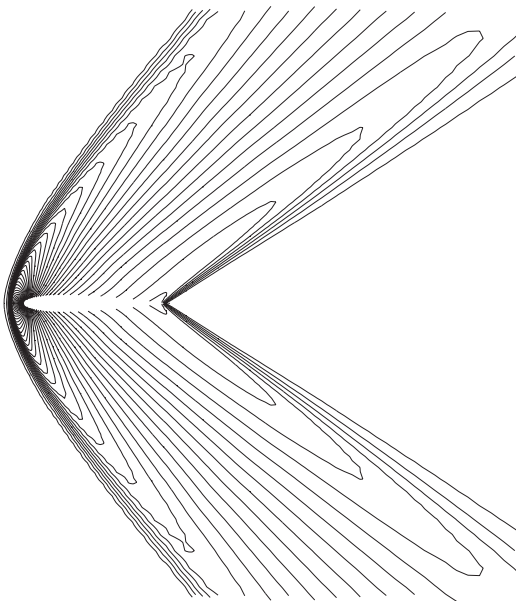

Figure 6. Mach contours ($M_\infty = 1.5$, rotational flow, $\alpha = 0^\circ$).

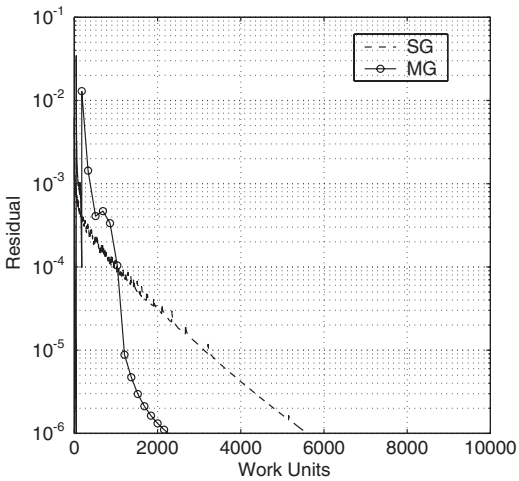

Figure 7. Convergence history ($M_\infty = 1.5$, potential flow, $\alpha = 0^\circ$).

2. PROBLEM FORMULATION: GOVERNING EQUATIONS AND BOUNDARY CONDITIONS

Consider a steady two-dimensional compressible flow over an airfoil. Following [5], the velocity vector can be decomposed into a gradient of a potential and a correction accounting

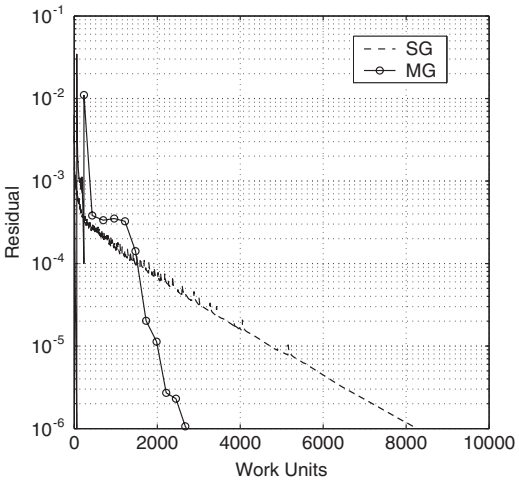

Figure 8. Convergence history ($M_\infty = 1.5$, rotational flow, $\alpha = 0^\circ$).

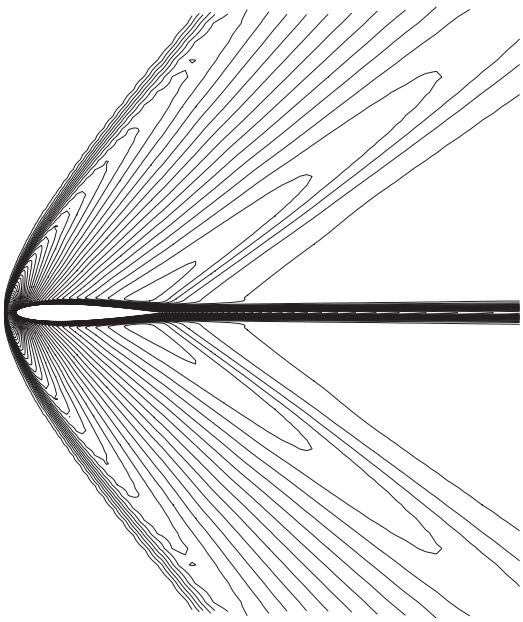

Figure 9. Mach contours ($M_\infty = 1.5$, $Re = 10\,000$, $\alpha = 0^\circ$) (coupling potential flow with a viscous layer).

for the rotational component, i.e.

$$\mathbf{q} = \nabla\phi + \mathbf{q}^* \tag{1}$$

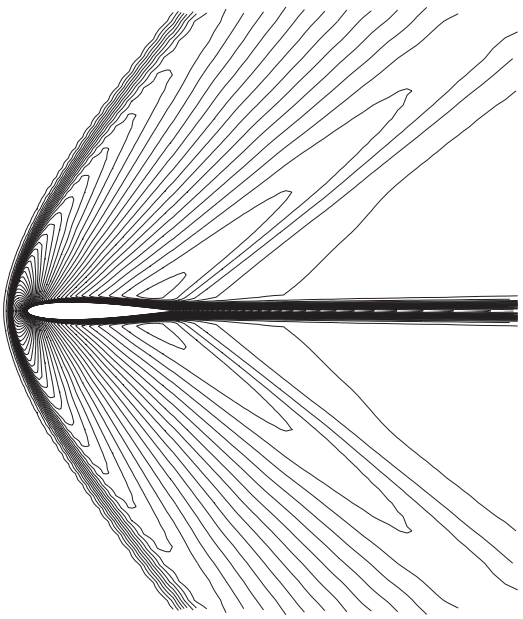

Figure 10. Mach contours ($M_\infty = 1.5$, $Re = 10\,000$, $\alpha = 0^\circ$) (coupling rotational flow with a viscous layer).

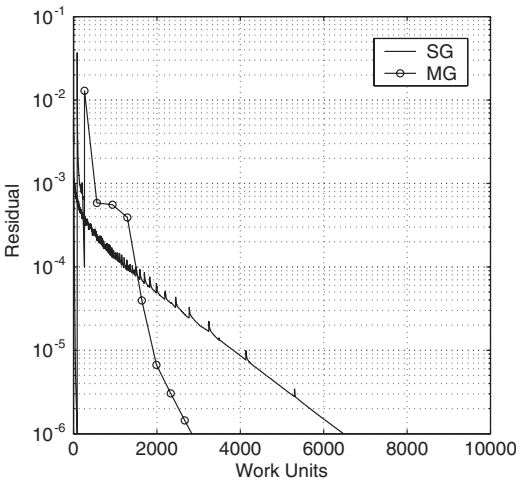

Figure 11. Convergence history ($M_\infty = 1.5$, $Re = 10\,000$, $\alpha = 0^\circ$) (coupling potential flow with a viscous layer).

The continuity equation, representing conservation of mass, can be written in the following form:

$$\nabla \cdot \rho \nabla \phi = -\nabla \cdot \rho \mathbf{q}^* \tag{2}$$

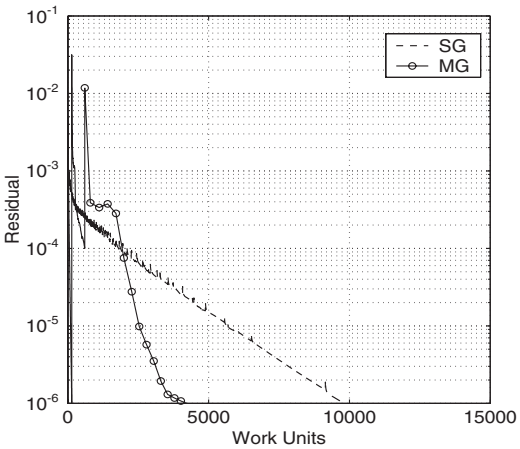

Figure 12. Convergence history ($M_\infty = 1.5$, $Re = 10\,000$, $\alpha = 0^\circ$) (coupling rotational flow with a viscous layer).

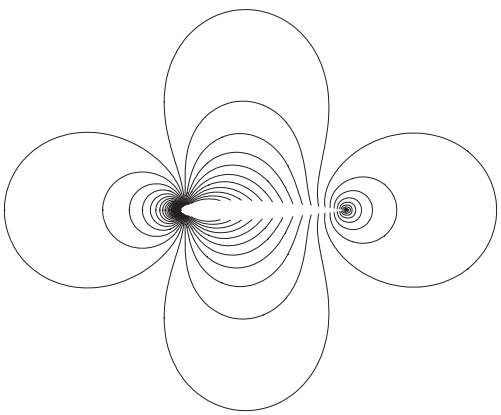

Figure 13. Mach contours ($M_\infty = 0.1$, potential flow, $\alpha = 0^\circ$).

In (2), the right-hand side is acting as a source term, or a forcing function. Equation (2) is solved with the no penetration boundary condition on the solid surface, i.e.

$$\frac{\partial \phi}{\partial n} = 0 \tag{3}$$

and a uniform flow with a potential vortex in the far field for lifting airfoils. The density in Equation (2) is calculated in terms of the speed augmented with an entropy correction

$$\rho = \rho_i \mathrm{e}^{-\Delta S/R} \tag{4}$$

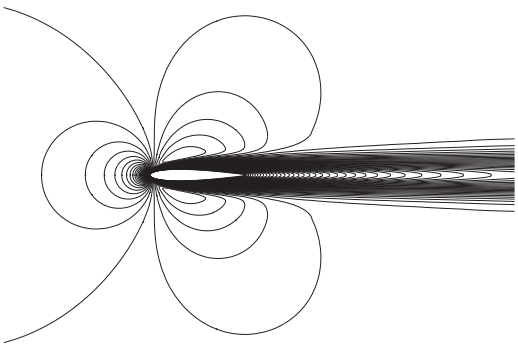

Figure 14. Mach contours ($M_\infty = 0.1$, $Re = 500$, $\alpha = 0^\circ$).

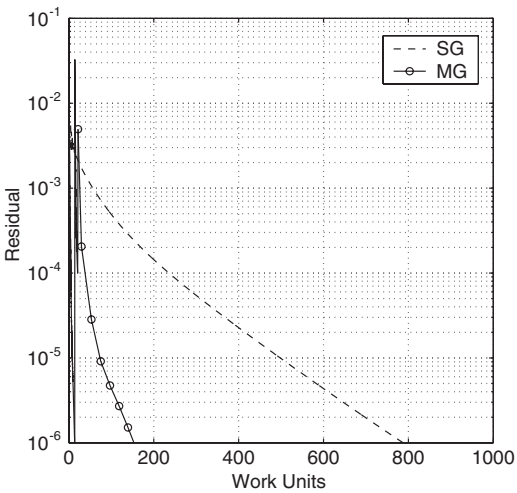

Figure 15. Convergence history ($M_\infty = 0.1$, potential flow, $\alpha = 0^\circ$).

where

$$\rho_i = \left[(\gamma - 1)M_\infty^2 \left(H - \frac{1}{2}q^2\right)\right]^{1/(\gamma-1)} \tag{5}$$

$$P = P_i \mathrm{e}^{-\Delta S/R}, \quad P_i = \frac{\rho_i^\gamma}{\gamma M_\infty^2} \tag{6}$$

H is the total enthalpy,

$$H = \frac{\gamma}{\gamma - 1}\frac{P}{\rho} + \frac{1}{2}q^2 = \frac{\gamma}{\gamma - 1}\frac{P_i}{\rho_i} + \frac{1}{2}q^2 \tag{7}$$

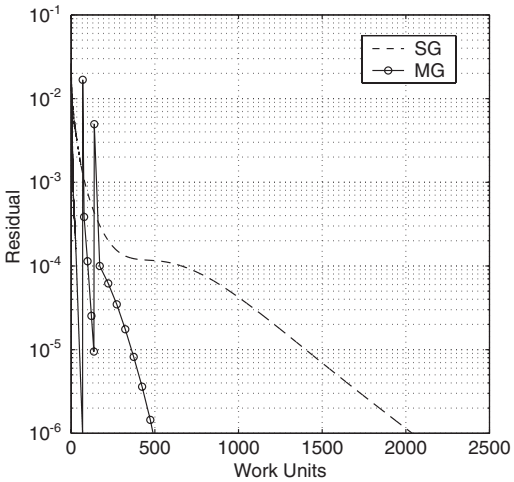

Figure 16. Convergence history ($M_\infty = 0.1$, $Re = 500$, $\alpha = 0^\circ$).

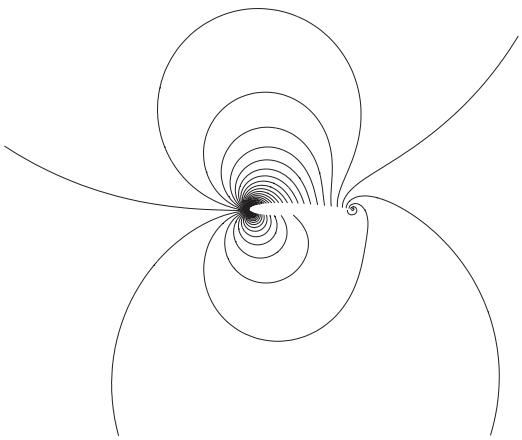

Figure 17. Mach contours ($M_\infty = 0.1$, potential flow, $\alpha = 10^\circ$).

The above formulation reduces to the standard potential equation for irrotational isentropic flows. The corrections due to entropy and vorticity are clearly represented by q^* and $e^{-\Delta S/R}$, respectively. The augmented potential equation is solved everywhere, while the corrections are usually limited to small regions for most aerodynamic flows.

The total enthalpy is assumed constant everywhere even in the viscous layer. This approximation is acceptable for compressible flows as discussed in Reference [5]. In general, the energy equation can be solved to provide H.

In the viscous layer, the speed (the magnitude of the velocity) is calculated from the tangential momentum equation, while the pressure (and hence the entropy) is calculated from the normal momentum equation. On the other hand, for inviscid rotational flows, the entropy

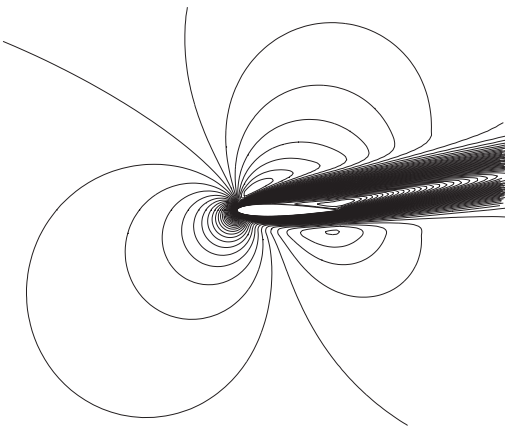

Figure 18. Mach contours ($M_\infty = 0.1$, $Re = 500$, $\alpha = 10^\circ$).

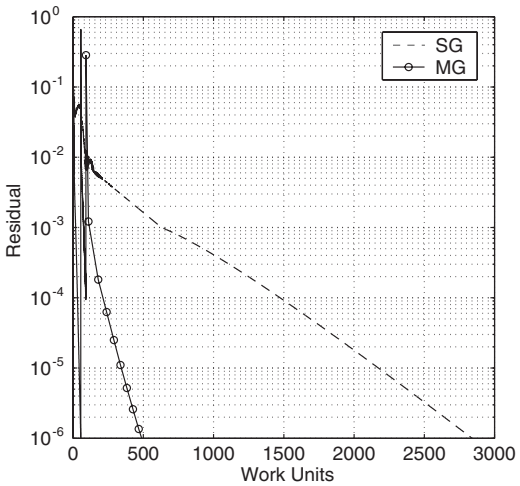

Figure 19. Convergence history ($M_\infty = 0.1$, potential flow, $\alpha = 10^\circ$).

generated from curved shocks is obtained from the balance of the tangential momentum and the rotational component of the velocity is calculated from Crocco's relation which is equivalent to the normal momentum equation. For more details, see Reference [5].

3. NUMERICAL METHODS

In this section, the grid, the scheme and the solver are briefly outlined. To discretize the domain, an algebraic grid generation is adopted. A C-grid is used as in Reference [5]. Finite volumes are chosen to discretize the equations, however, finite elements can be used as well.

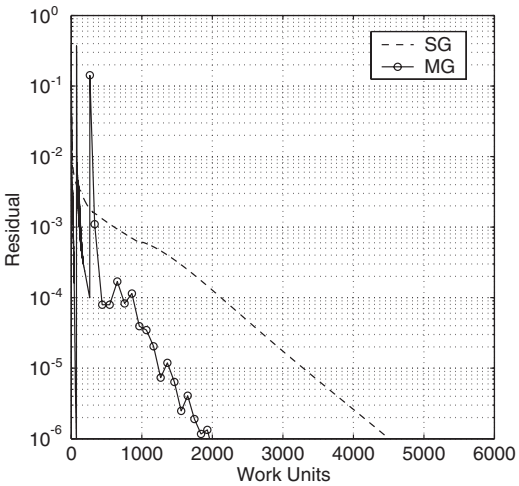

Figure 20. Convergence history ($M_\infty = 0.1$, $Re = 500$, $\alpha = 10^\circ$).

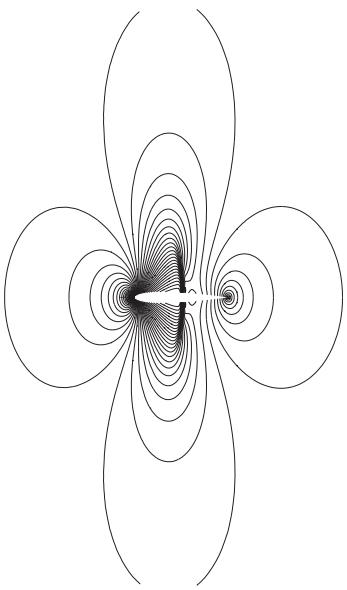

Figure 21. Mach contours ($M_\infty = 0.8$, potential flow, $\alpha = 0^\circ$).

Artificial time-dependent terms are added to the momentum equations to help the overall convergence. Artificial viscosity is needed for numerical stability for the potential equation in the supersonic region and for the convection terms in the momentum equations. Deferred correction approach is implemented where the original equations are written in conservation forms.

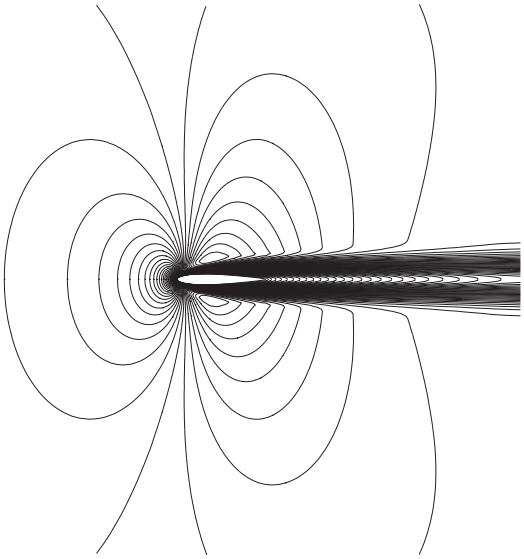

Figure 22. Mach contours ($M_\infty = 0.8$, $Re = 500$, $\alpha = 0^\circ$).

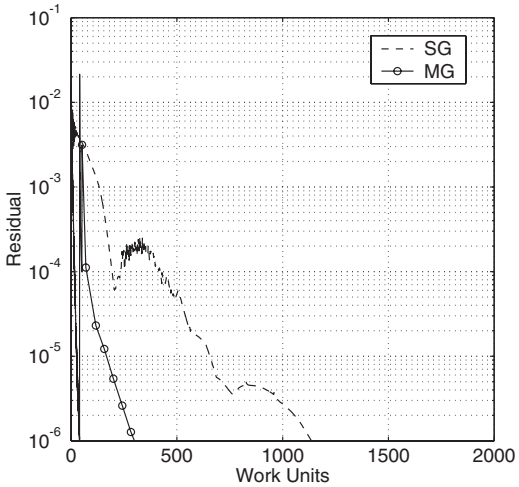

Figure 23. Convergence history ($M_\infty = 0.8$, potential flow, $\alpha = 0^\circ$).

The multigrid acceleration techniques are used only for the augmented potential equation. The momentum equations are solved only on the fine mesh. This simple strategy is a very convenient way to avoid many problems associated with high speed flows. The restriction of multigrid application to the potential equation may not, however, provide the optimal convergence rate and other strategies dealing with the convection/diffusion equations will be studied elsewhere.

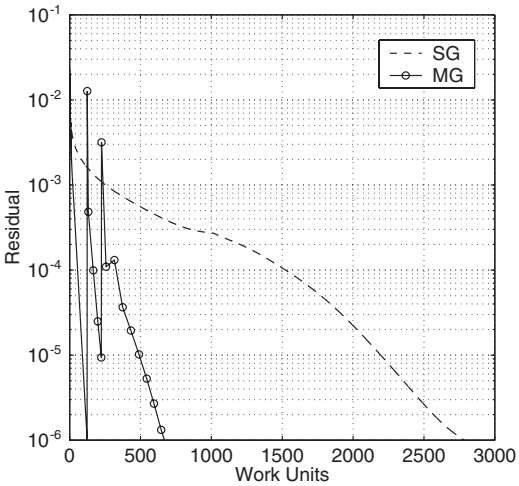

Figure 24. Convergence history ($M_\infty = 0.8$, $Re = 500$, $\alpha = 0^\circ$).

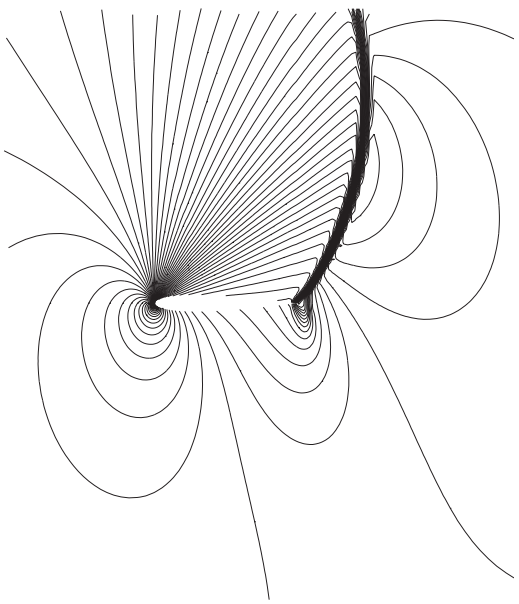

Figure 25. Mach contours ($M_\infty = 0.8$, potential flow, $\alpha = 10^\circ$).

The present formulation allows easily the identification of the acoustic mode represented by the potential equation, while the entropy and vorticity modes are governed by scalar convection/diffusion equations. For many transonic aerodynamic problems, most of the near and far flow fields are subsonic, hence an effective treatment of the elliptic potential equation is very attractive. On the other hand, for standard Euler and Navier–Stokes equations, the

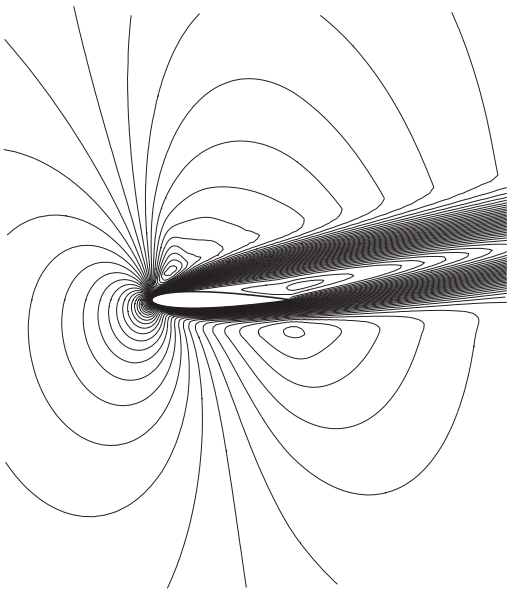

Figure 26. Mach contours ($M_\infty = 0.8$, $Re = 500$, $\alpha = 10^\circ$).

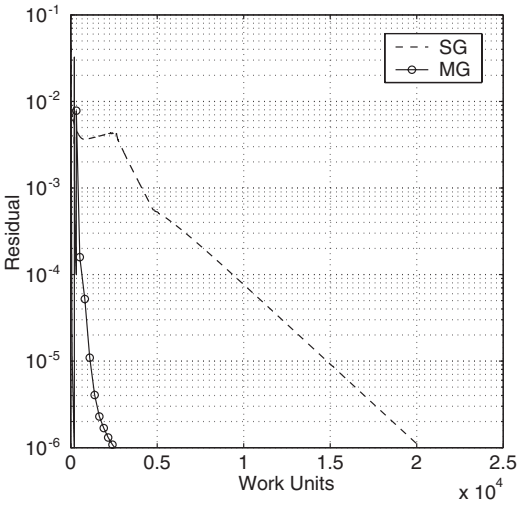

Figure 27. Convergence history ($M_\infty = 0.8$, potential flow, $\alpha = 10^\circ$).

identification of the modes are not obvious nor simple in general. Many attempts to exploit the structure of certain schemes to achieve splitting of the modes on the discrete level are encouraging but usually there are restrictions on the grid and calculations are more complicated.

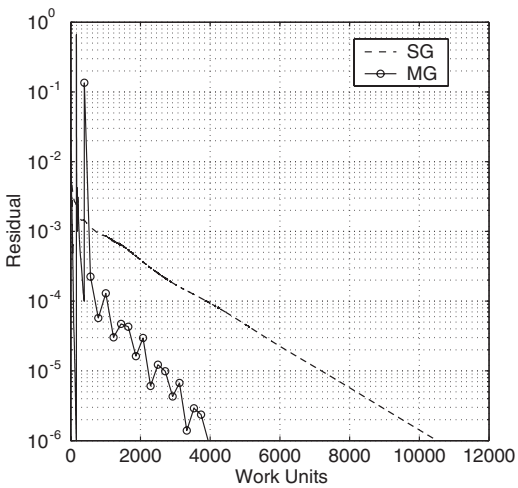

Figure 28. Convergence history ($M_\infty = 0.8$, $Re = 500$, $\alpha = 10^\circ$).

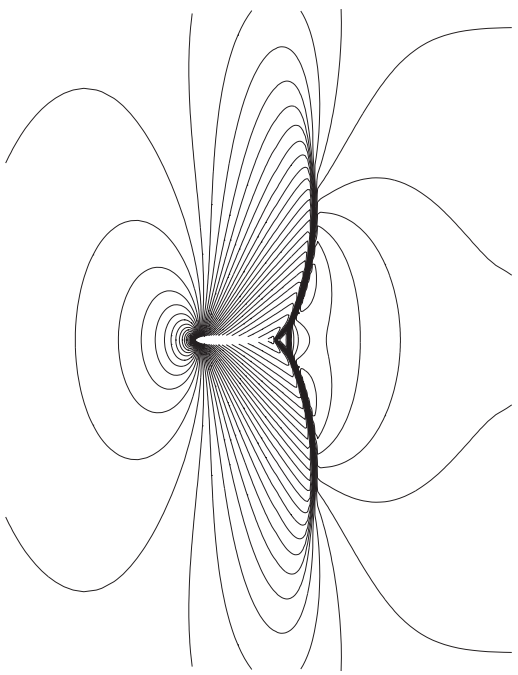

Figure 29. Mach contours ($M_\infty = 0.9$, potential flow, $\alpha = 0^\circ$).

A type dependent line relaxation procedure with optimal parameters is used for single grid calculations for comparison. An order of magnitude reduction in work units is possible with the present multigrid acceleration. Full weighting for restriction and bilinear interpolation for prolongation are implemented in a straightforward manner.

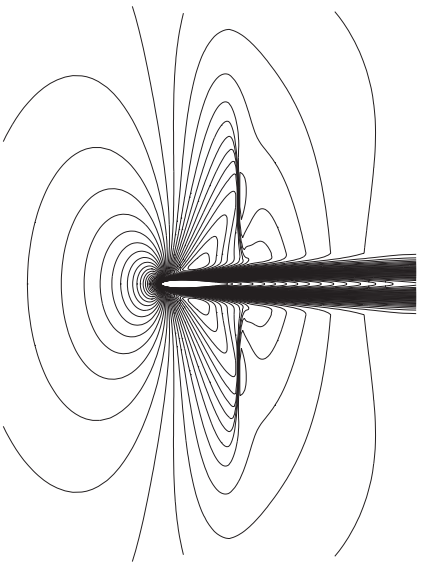

Figure 30. Mach contours ($M_\infty = 0.9$, $Re = 500$, $\alpha = 0^\circ$).

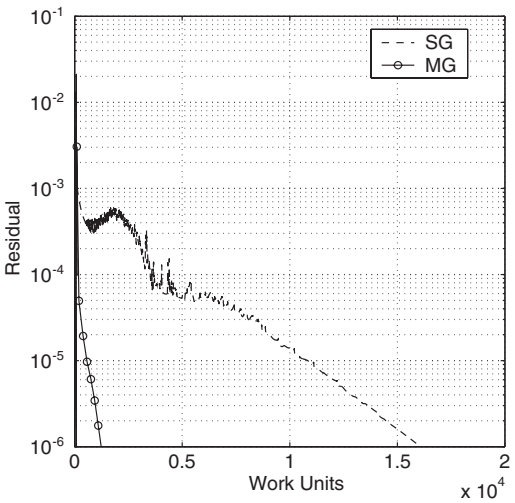

Figure 31. Convergence history ($M_\infty = 0.9$, potential flow, $\alpha = 0^\circ$).

To discuss the process, consider only two grids, coarse and fine. If the residual on the fine mesh is $R_f(\phi_f)$, the restriction on the coarse mesh is denoted by $CR_f(\phi_f)$. For linear problems, $R_f(\phi_f) = A_f\phi_f - b_f$, one can obtain the correction on the coarse mesh from

$$A_c(\delta\phi_c) = -CR_f(\phi_f) \tag{8}$$

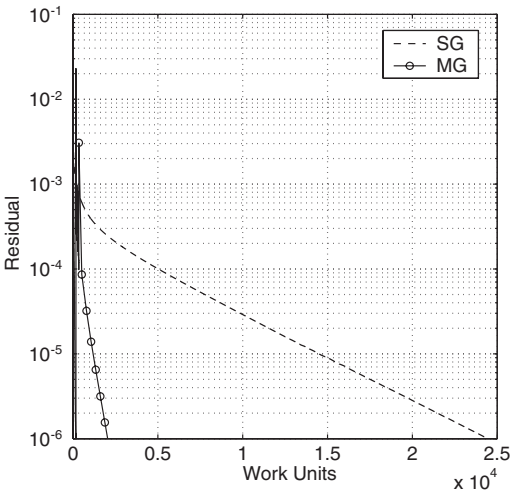

Figure 32. Convergence history ($M_\infty = 0.9$, $Re = 500$, $\alpha = 0^\circ$).

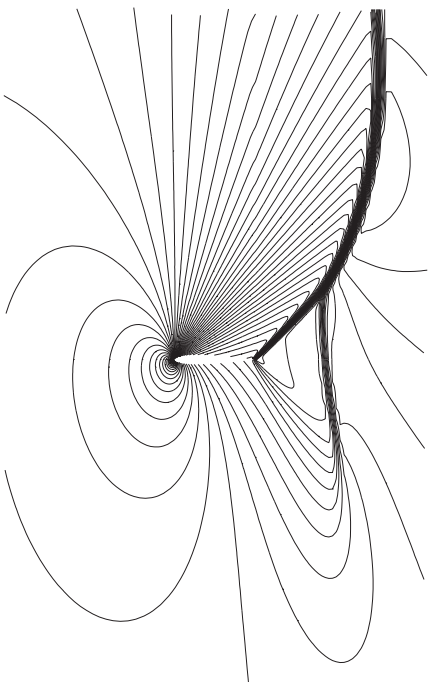

Figure 33. Mach contours ($M_\infty = 0.9$, potential flow, $\alpha = 10^\circ$).

The correction on the fine mesh is calculated from

$$\delta\phi_f = P\delta\phi_c \tag{9}$$

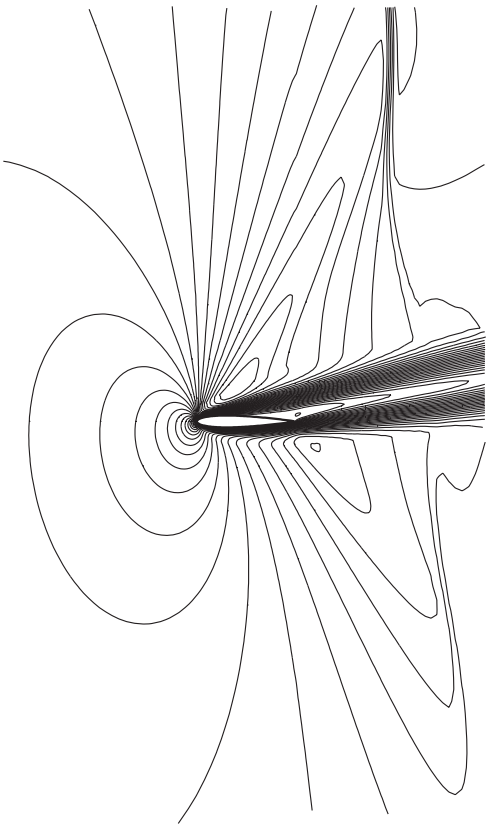

Figure 34. Mach contours ($M_\infty = 0.9$, $Re = 500$, $\alpha = 10^\circ$).

where P stands for the prolongation operator (in principle; $PC = CP = I$). Following Brandt and Jameson, for non-linear problems, a full approximation scheme (FAS) is applied where Equation (8) is modified to read

$$R_c(\phi_c) = R_c(C\phi_f) - CR_f(\phi_f) \tag{10}$$

The right-hand side of Equation (10) is the difference between the residual on the coarse mesh, evaluated based on the restriction of the fine mesh values ϕ_f, and the restriction of the fine mesh residual to the coarse mesh. In solving Equation (10) on the coarse mesh, the right-hand side should be frozen. A correction on the coarse mesh from the solution of Equation (10) can be calculated from

$$(\delta\phi_c) = \phi_c - C\phi_f \tag{11}$$

The correction on the fine mesh is obtained by prolongation, hence the fine mesh solution is

$$(\phi_f)_{new} = (\phi_f)_{old} + P(\delta\phi_c) \tag{12}$$

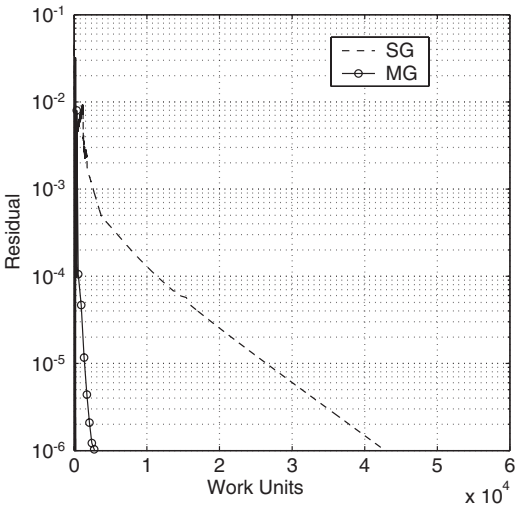

Figure 35. Convergence history ($M_\infty = 0.9$, potential flow, $\alpha = 10^\circ$).

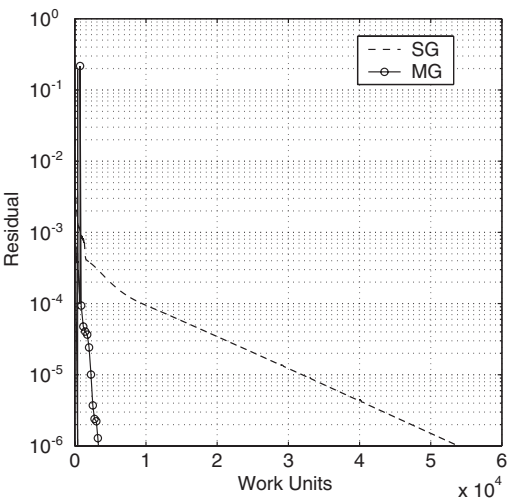

Figure 36. Convergence history ($M_\infty = 0.9$, $Re = 500$, $\alpha = 10^\circ$).

Few iterations on the fine mesh are needed to smooth high-frequency errors resulting from interpolation. The above process can be extended to more than two grids by induction. In the present calculations, only three grids are used and the solution is fully converged on the coarsest mesh. Programming multigrid, in general, is not simple, and there are many available references full of details.

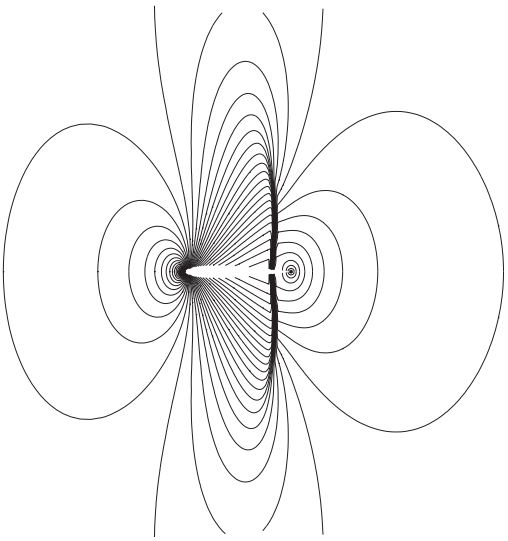

Figure 37. Mach contours ($M_\infty = 0.85$, potential flow, $\alpha = 0^\circ$).

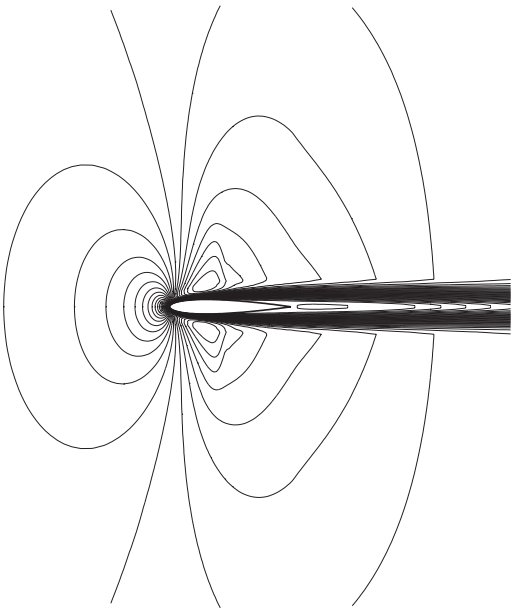

Figure 38. Mach contours ($M_\infty = 0.85$, $Re = 2000$, $\alpha = 0^\circ$).

4. NUMERICAL RESULTS

Several cases are calculated for transonic flows over NACA0012 airfoil at different angles of attack, Mach and Reynolds numbers. These cases include: potential flows, inviscid rotational

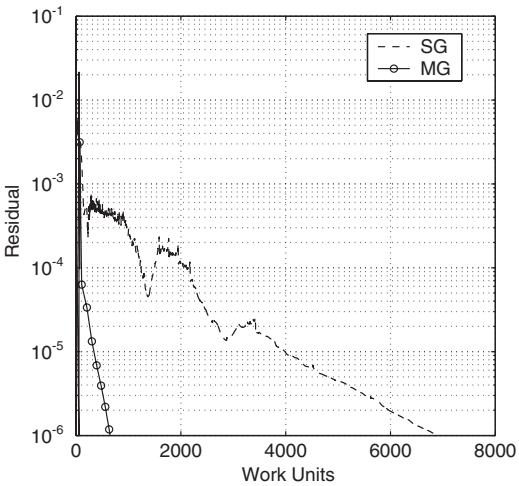

Figure 39. Convergence history ($M_\infty = 0.85$, potential flow, $\alpha = 0^\circ$).

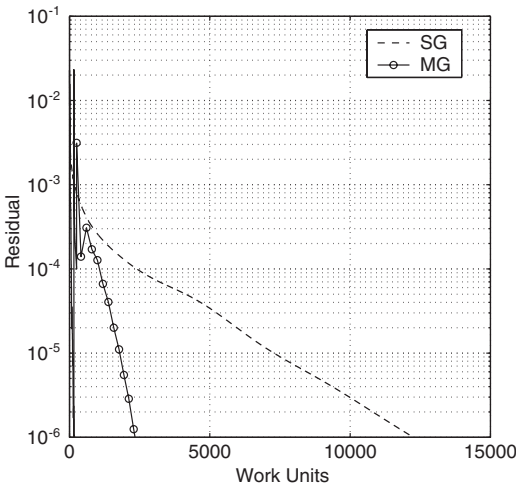

Figure 40. Convergence history ($M_\infty = 0.85$, $Re = 2000$, $\alpha = 0^\circ$).

flows and viscous flows. The residual histories for single and multiple grids are compared for each case.

4.1. Inviscid rotational flows

Figures 1 and 2 show the Mach contours for potential and inviscid rotational flows at $M_\infty = 0.86$ and $\alpha = 0^\circ$. The corresponding convergence histories are plotted in Figures 3 and 4. Notice that the convergence rates of the potential and rotational flows are very similar for single and multiple grids.

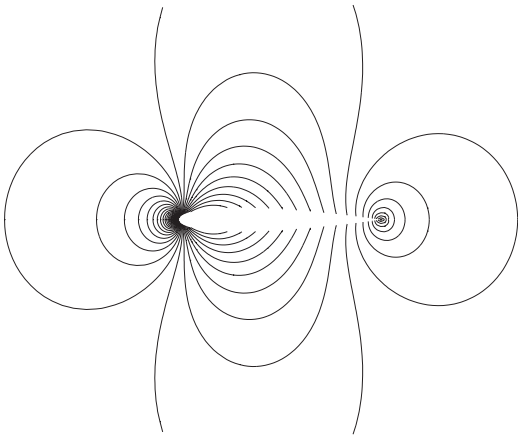

Figure 41. Mach contours ($M_\infty = 0.5$, potential flow, $\alpha = 0^\circ$).

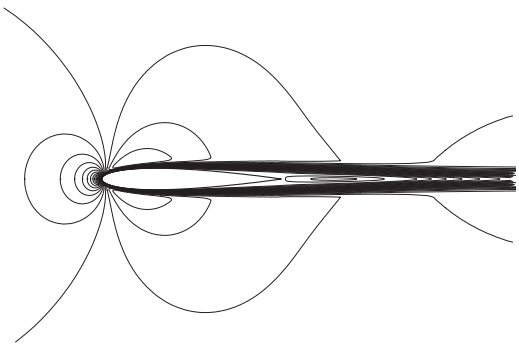

Figure 42. Mach contours ($M_\infty = 0.5$, $Re = 10\,000$, $\alpha = 0^\circ$).

Similar results for $M_\infty = 1.5$ and $\alpha = 0^\circ$ are plotted in Figures 5–8. The corresponding results for viscous supersonic flow calculations ($Re = 10\,000$), with and without including the entropy and the vorticity generated by curved shocks, are shown in Figures 9–12.

4.2. Viscous flows

In Figures 13 and 14, the Mach contours are plotted for potential and viscous flows ($Re = 500$) at $M_\infty = 0.1$ and $\alpha = 0^\circ$. The corresponding residual histories are plotted in Figures 15 and 16. Similar results for the case of $\alpha = 10^\circ$ are shown in Figures 17–20. In these calculations, the compressibility effects are minimal. The present formulation includes the incompressible flow limit as discussed in Reference [5].

The results for $M_\infty = 0.8$ and $M_\infty = 0.9$ at $\alpha = 0$ and 10° for potential and viscous flows ($Re = 500$) are plotted in Figures 21–36. The results for $M_\infty = 0.85$ at $\alpha = 0^\circ$ for potential and viscous flows ($Re = 2000$) are plotted in Figures 37–40. The work unit for viscous flow simulations includes the residual evaluations of the augmented potential equation

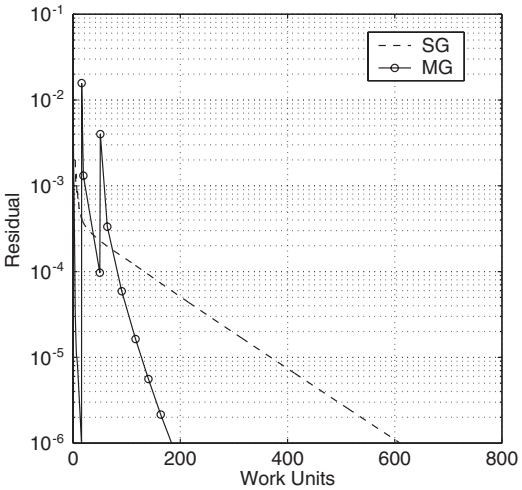

Figure 43. Convergence history ($M_\infty = 0.5$, potential flow, $\alpha = 0^\circ$).

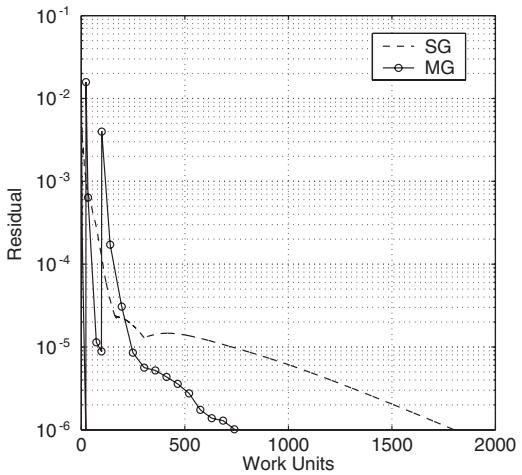

Figure 44. Convergence history ($M_\infty = 0.5$, $Re = 10\,000$, $\alpha = 0^\circ$).

and the momentum equations on the fine mesh. The latter are updated only in the viscous layer.

Higher Reynolds number flows ($Re = 10\,000$) are calculated for $M_\infty = 0.5$ at $\alpha = 0^\circ$, see Figures 41–44. For these cases, a highly stretched grid is used without noticeable degeneration of multigrid performance. The above numerical results are in good agreement with those available in the literature for the same test cases, see References [8, 9].

5. CONCLUDING REMARKS

Multigrid techniques are applied to accelerate the convergence of transonic aerodynamic flow simulations based on a hierarchical formulation for both inviscid and viscous flows. For both cases, the augmented potential equation is solved using iterative methods and the gain of multigrid acceleration is substantial. An order of magnitude reduction in the work unit is achieved for some of the test cases. For supersonic free streams, the present application of multigrid is not as impressive. More sophisticated strategies should achieve further savings. Extensions to three dimensional flows are feasible.

REFERENCES

1. Brandt A. *Multigrid Techniques: 1984 Guide with Applications to Fluid Dynamics*, GMD-Studie, vol. 85. GMD-FIT, 1985.
2. Thomas JL, Diskin B, Brandt A. Textbook multigrid efficiency for fluid simulations. *Annual Review of Fluid Mechanics* 2003; **35**:317–340.
3. Caughey DA, Jameson A. Fast preconditioned multigrid solution of the Euler and Navier–Stokes equations for steady compressible flows. *International Journal for Numerical Methods in Fluids* 2003; **43**:537–553.
4. Jameson A. Solution of the Euler equations for two-dimensional, transonic flow by a multigrid method. *Applied Mathematics and Computation* 1983; **13**:327–356.
5. Hafez M, Wahba E. Numerical simulations of transonic aerodynamic flows based on a hierarchical formulation. *International Journal for Numerical Methods in Fluids*, this issue.
6. Jameson A. Accelerations of transonic potential flow calculations on arbitrary meshes by the multiple grid method. *AIAA Paper 79-1458*, 1979.
7. Drikakis D, Iliev O, Vassileva D. On multigrid methods for the compressible Navier–Stokes equations. *ICLSSC 2001*. Springer: Berlin, 2001; 344–352.
8. Hollanders H, Lerat A, Peyert R. 3-D calculations of transonic viscous flows by an implicit method. *AIAA Paper 83-1953*, 1983.
9. Hafez MM, Guo WH. Simulation of steady compressible flows based on Cauchy/Riemann equations and Crocco's relation, Part II: viscous flows. *International Journal for Numerical Methods in Fluids* 1999; **31**:325–343.

